

Optimal Trajectory Control of an Occulter-Based Planet-Finding Telescope

Egemen Kolemen* and N. Jeremy Kasdin *

Princeton University, Princeton, NJ, 08544, USA

The optimal configuration of a satellite formation consisting of a telescope and an occulter around Sun-Earth L2 Halo orbits is studied. Trajectory optimization of the occulter motion between imaging sessions of different stars is performed using a range of different criteria and methods. For the direct optimization method, an automated algorithm is written, which converts the optimal control problem to a discrete optimization problem. This is then solved using a Sequential Quadratic Programming (SQP) algorithm. Thus, the global optimization problem is transformed into a Time-Dependent Traveling Salesman Problem (TSP). The TSP is augmented with various constraints that arrive from the mission, and this problem is solved employing Tabu Search and Branch-And-Cut algorithms. For a concrete understanding of the feasibility of the mission, the performance of an example spacecraft, SMART-1, is analyzed.

I. Introduction

It is likely that the next decade will see NASA launch the first in a series of missions dubbed the Terrestrial Planet Finders (TPF) to detect, image, and characterize extrasolar earthlike planets. Current work is directed at studying a variety of architecture concepts and the associated optical engineering in order to prove the feasibility of such a mission. One such concept involves the formation flying of a conventional space telescope on the order of 2 to 4 meter diameter, in a Sun-Earth L2 Halo orbit, with a large occulter, roughly 30 m across and 50,000 km away, to block the light of a star and allow imaging of its dim, close-by planetary companion. Recent results in shaped-pupil technology at Princeton have made the manufacture of such a starshade feasible.^{1,2} This approach to planet imaging eliminates all of the precision optical requirements that exist in the alternate coronagraphic or interferometric approaches. However, it introduces the difficult problem of controlling and realigning the satellite formation.

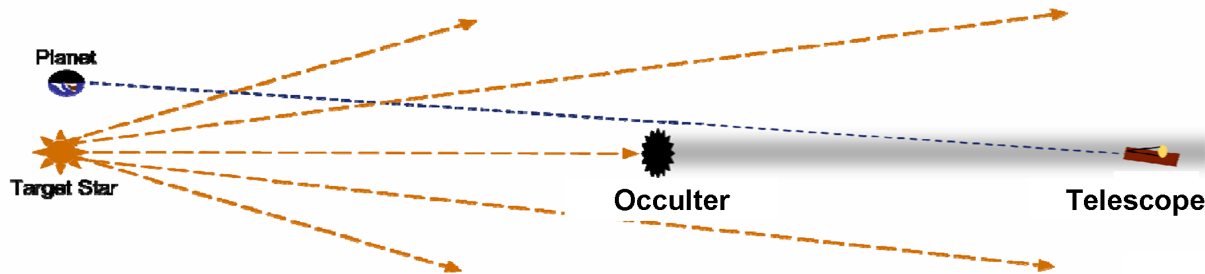


Figure 1. Occulter-based extra-solar planet-finding mission diagram³

In this paper, we study the optimal configuration of satellite formations consisting of a telescope and an occulter. The objective is to enable the imaging of the largest possible number of planetary systems with minimum mass requirement which consists of the dry mass of the spacecraft and the total fuel requirement for the formation. As we use more control, scientific achievement, that is, the number of planetary systems

*ekolemen@princeton.edu, Mechanical and Aerospace Engineering Department, Princeton, NJ, 08544, USA.

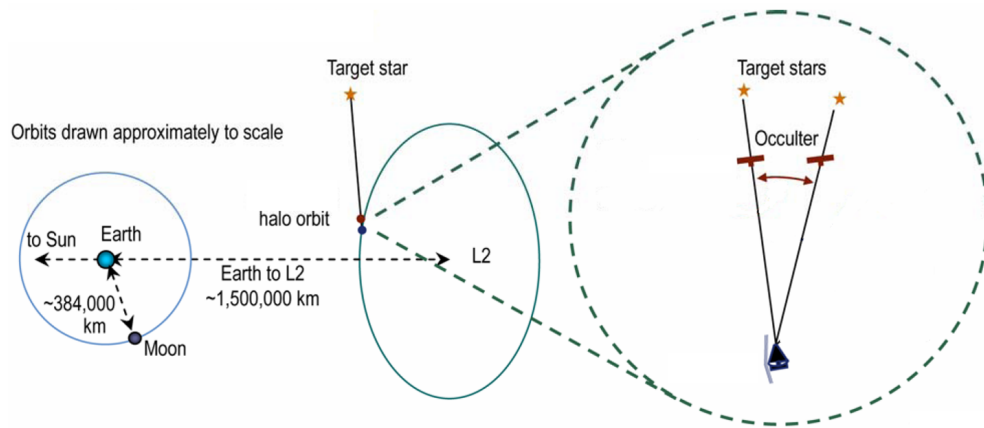


Figure 2. A schematic diagram of occulter mission orbits projected into the ecliptic plane³

that are imaged, is higher but so is the cost due to thruster weight and fuel consumption. This paper enables a trade-off study, using different thrusters and imaging different star systems in terms of cost and scientific achievement.

The control problem can be separated into two parts; first, the line-of-sight (LOS) control of the formation during imaging, and second, the trajectory control for realignment between imaging sessions. Realignment is far more dominant in fuel consumption than LOS control. We therefore focus on the realignment problem to get an estimate of the total fuel consumption.

First, the optimal control problem of the realignment is solved. This gives us the minimum energy and minimum time trajectories that take the occulter from a given star LOS to another LOS. The solution to the optimal control problem is implemented using three different methodologies. First, a Lambert-like approach is employed, where the control consists of two large Delta-V maneuvers at the beginning and at the end of the trajectory. The second approach, the direct method, is to discretize the optimal control problem and solve a high-dimensional nonlinear optimization problem via a SQP method. The third approach, the indirect method, uses the Euler-Lagrange formulation, i.e. the adjoint method, in order to find a continuous thrust solution. This method is very fast, thus enabling millions of trial cases to be solved. This reduces the Delta-V solution of the dynamical optimization problem to an approximate function of the major parameters of the problem such as the time-to-go, the angular separation, and the distance between the telescope and the occulter. All three methods are applied, and the results of each method are compared with one another.

To minimize the time it takes to convert the optimal control problem to a form that can be used with the direct method, an automated symbolic software is created. This algorithm discretizes the optimal control problem, which is defined effortlessly in MATLAB. It then converts it to FORTRAN and "mex"es this code back to MATLAB. This allows us to solve the problem without leaving the convenience of the MATLAB environment while having the speed of the FORTRAN's fast compiler. The authors hope to make this software available for the public soon.

After finding the relevant minimum-fuel trajectories between all the target stars, the sequencing and timing of the imaging session is examined in order to minimize global fuel consumption. By including the constraints imposed by the telemetry requirements, the problem becomes a Dynamic Time-Dependent Traveling Salesman Problem with dynamical constraints. Branch-And-Cut and Tabu Search heuristic methods are employed to solve the Traveling Salesman Problem (TSP).

In this paper, we focus on the single occulter formation around a telescope. For a further study on the control of a constellation of multiple occulters, which is based on the methods developed in this paper, see Kolemen & Kasdin.⁴

For a concrete understanding of the feasibility of the mission, we look at possible mission scenarios using current technology. To this end, the performance of an example spacecraft, SMART-1, is analyzed.

These results give an approximate Delta-V budget for different configurations, which will be useful for a trade-off study of various spacecraft control systems and strategies, as well as target selection.

II. Optimization of the Mission

In Kolemen & Kasdin,⁵ the dynamics around the Sun-Earth L2 point is analyzed with a focus on the periodic and quasi-periodic orbits. For the mission of interest, where the telescope resides on a Halo orbit, Quasi-Halo orbits are fuel-free trajectories with favorable properties where the occulter may be placed. Figure 4 shows an example of the relative motion of an occulter placed on a Quasi-Halo orbit, with respect to the telescope on a Halo orbit. As seen in the figure, the occulter covers the full sky, which makes possible the imaging of all the target stars. This is done without any fuel consumption, and while keeping the distance approximately fixed, since the Quasi-Halo orbits are part of the dynamical structure around the L2 libration point, which enables the spacecraft to ride the wave. However, a major drawback of placing a spacecraft on a Quasi-Halo orbit is that the periods of these orbits around the Halo are roughly 6 months. As a result, a single spacecraft located on a Quasi-Halo orbit will not be able to fulfill the requirement of imaging a target approximately every 1 to 2 weeks.

There are two possible approaches to this problem. The first approach employs a single occulter with fuel-intensive trajectory control, while the second one employs multiple occulters that use the natural dynamics more efficiently, thus minimizing fuel consumption per spacecraft. While employing multiple spacecraft increases the mission's total mass, because of the duplication of all the components, it reduces the maximum thrust, which enables us to use smaller thrusters, and which reduces the mass per spacecraft. In addition, redundancy in the multiple spacecraft system will be an insurance in case of a malfunctioning of one of the occulter systems. In this paper, we focus on the single occulter formation with optimal control. For further study of the best configuration of a constellation consisting of multiple occulters based on the methods developed in this paper, see Kolemen & Kasdin.⁴

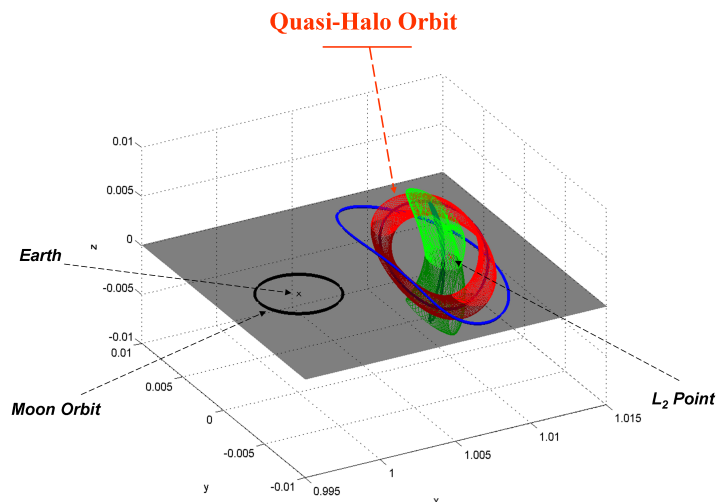


Figure 3. All the periodic and quasi-periodic orbits around the L2 point. The Quasi-Halo orbits, which form a torus around the Halo orbit, are highlighted.

The control problem can be separated into two parts; first, the line-of-sight (LOS) control of the formation during imaging, and second, the trajectory control for maneuvering the occulter from one star LOS to another between imaging sessions, i.e., the realignment process. Here we focus on the latter, since the realignment dominates the Delta-V budget. This study is done in two sections. In the first section, we find the minimum Delta-V need for the realignment processes. Subsequently, the sequencing and timing of the imaging session is examined in order to minimize global fuel consumption.

This section aims to arrive at the algorithms that optimize the different mission scenarios from beginning to end, and that reduce the complexities of the various missions to simple graphs, where the side-by-side comparison of the advantages and disadvantages of these missions is possible. This makes possible a trade-off study, using different control strategies, in terms of cost, i.e. the total Delta-V for the mission, and scientific achievement, i.e. the number of planetary systems that are imaged.

For ease of comparison, all the missions scenarios discussed from here on assume a base Halo orbit around

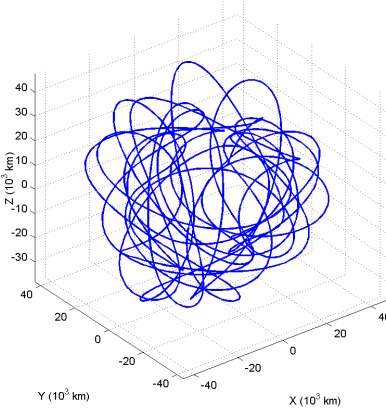


Figure 4. Relative position of the occulter placed on a Quasi-Halo orbit with respect to the telescope on a Halo orbit in the inertial frame (Mean Radius = 30,000 km)

L2 with an out-of-plane amplitude of 500,000 km.

III. Finding the Delta-V for the Realignment Between Imaging Sessions

We look at four optimization strategies for the realignment. The first strategy assumes that the thrust is applied impulsively at the beginning and at the end of the maneuver. The second presupposes continuous thrust between two given star LOS's with a given time of flight. The third option presumes continuous thrust and knowledge of the initial condition but not the end point. The last optimization is the type of maneuver where the time of flight is unknown but a constraint on the maximum thrust exists. In the following sections, we go over these four different optimization strategies, and we discuss the approaches taken to solve the optimal control problem that arises from these different assumptions. However, we first review the general optimal control methods.

In this study, we employed the full nonlinear model given by JPL DE-406 ephemeris⁶ for differential equations and performed the exact star location conversions to the body frame in order to obtain high fidelity. Simplified models, such as the Restricted Three-Body Problem, and a uniformly rotating star model are employed for low-order faster calculations.

A. The Euler-Lagrange Formulation of the Optimal Control Problem (Indirect Method)

The Euler-Lagrange method, otherwise known as the adjoint method, employs the variational calculus to find the optimal control of a differential system. Here we only outline the methodology; for details see Bryson and Ho.⁷

Given a function J to minimize,

$$J = \phi(x_f) + \int_{t_0}^{t_f} L(t, x, u) dt \quad (1)$$

subjected to ordinary differential equations,

$$\dot{x} = f(t, x, u) \quad \& \quad \beta(t_f) = 0 \quad (2)$$

Euler-Lagrange equations give the optimal solution path as a Boundary Value Problem (BVP) in terms of the augmented state consisting of the normal states and adjoint-states (λ).

$$\dot{x} = f(t, x, u) \quad (3)$$

$$\dot{\lambda} = -H_x^T(t, x, u, \lambda) \quad (4)$$

$$0 = H_u(t, x, u, \lambda). \quad (5)$$

These equations are subjected to the following boundary conditions:

$$\lambda_f = G_{x_f}^T(x_f, \nu) \quad \& \quad \beta(x_f) = 0. \quad (6)$$

In these equations H (the Hamiltonian) and G are given as

$$H = L(t, x, u) + \lambda^T f(t, x, u) \quad \& \quad G = \phi(x_f) + \nu^T \beta(x_f). \quad (7)$$

The main advantage of using the Euler-Lagrange formulation is that the optimality of the solution can be checked, and that the computational effort will be minimal if a feasible solution can be found. The main disadvantage is that it may be difficult to formulate initial guesses for the adjoint states.

B. The SQP Formulation of the Optimal Control Problem (Direct Method)

The second approach is to discretize the optimal control problem and solve a high-dimensional nonlinear optimization problem via a SQP algorithm. Since there are no intermediate steps involved in solving the problem, this method is called the direct method.

$$t_{initial} = t_0 < t_1 \dots < t_{N-1} < t_N = t_{final}. \quad (8)$$

We approximate the state and control at each time point $x_i = x(t_i)$, $u_i = u(t_i)$. If our guess is sufficiently close to the real solution, the discretized quadrature equation, which corresponds to the differential equation, gives the following constraint at every point for the trapezoidal discretization:

$$0 = \Phi(t_i, x_i, u_i) = -x_{i+1} + x_i + h_i (f(t_i, x_i, u_i) + f(t_{i+1}, x_{i+1}, u_{i+1})). \quad (9)$$

where

$$h_i = t_{i+1} - t_i. \quad (10)$$

There are many other discretization schemes; the trapezoidal is used here for illustration. Along with the differential equation, the cost function and the constraints, if the latter exist, are discretized as well.

$$J = \phi(x_f) + \sum_{i=0}^{i_f} L(t_i, x_i, u_i) dt \quad (11)$$

Once the high-dimensional discrete nonlinear optimization problem is formed, it is solved via a SQP algorithm. For this purpose, LOQO⁸ and IPOPT⁹ interior method SQP-solver software are utilized.

To minimize the time it takes to convert the optimal control problem to a form that can be used with the direct method, an automated symbolic software is created. This algorithm discretizes the optimal control problem, which is defined effortlessly in MATLAB. It then converts it to FORTRAN and "mex"es this code back to MATLAB. This allows us to solve the problem without leaving the convenience of the MATLAB environment while having the speed of the FORTRAN's fast compiler. Many different discretization methods such as Runge-Kutta, Euler, and trapezoidal are available to suit the needs of the specific problem. The authors hope to make this software available for the public soon.

C. Four Different Optimal Control Approaches

1. The Impulsive Thrust Case

During the imaging of a given planetary system, the telescope and the occulter must be aligned to lock to the LOS of the star position. Thus, the inertial velocities of the telescope and the occulter should be the same. In addition, for optical purposes, the distance between the occulter and the telescope should be roughly the same for all observations. This fixes the position of the occulter to be on a sphere around the telescope. The problem then becomes one of finding an optimal trajectory between two, two-dimensional surfaces, as shown in figure 5.

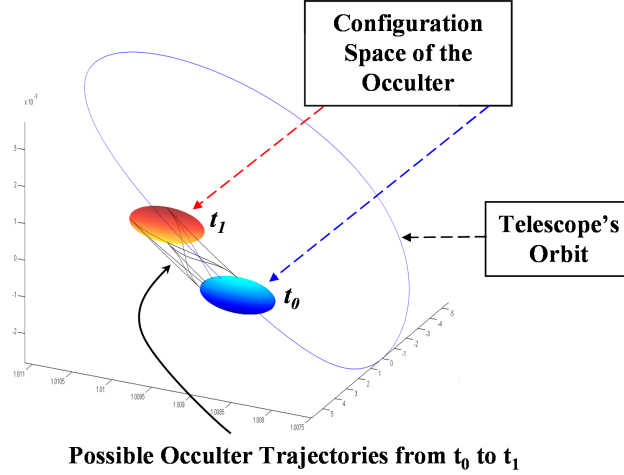


Figure 5. The sphere of possible occulter locations about the telescope at two times, and example optimal trajectories connecting them

First, we look at the optimal control problem of finding the trajectory that takes the occulter from the first star LOS to the second LOS. A Lambert-like approach is employed, where the control consists of two large Delta-V maneuvers at the beginning and at the end of the trajectory. This control changes the velocity of the occulter while keeping the position constant. Thus, the objective is to find the velocities at the initial time, t_0 , and the final time, t_f , given the initial and final positions. The Delta-V will be the difference between the computed velocity and the required velocity for planetary system observation. Mathematically, the problem is to solve for the 3 unknown velocities at both boundary points, a total of 6 unknowns, given the 3 known positions at both boundary points. This is a well-posed BVP and can be solved using various methods such as shooting, multiple-shooting and collocation. In our research, we employ a collocation algorithm.

2. The Continuous Point-to-Point Case

As this is the first case, a detailed explanation will be given. The following cases are explained more briefly. Our aim is to minimize the control effort given the differential equations of motion.

$$L(t, x, u) = \frac{1}{2}(u_1^2 + u_2^2 + u_3^2) \quad \& \quad f(t, x, u) = f(t, x) + [0; 0; 0; u_1; u_2; u_3] \quad (12)$$

In this point-to-point optimal control, both the initial and final states are fixed a priori.

$$\beta(t_f) = \mathbf{x}(t_f) - \mathbf{x}_f = 0 \quad (13)$$

Solving the optimality condition,

$$0 = H_u(x, u, \lambda) \quad (14)$$

we obtain,

$$\begin{pmatrix} u_1 \\ u_2 \\ u_3 \end{pmatrix} = - \begin{pmatrix} \lambda_4 \\ \lambda_5 \\ \lambda_6 \end{pmatrix}. \quad (15)$$

replacing control with the adjoint variables, we get a 12 dimensional BVP

$$\dot{x} = f(t, x, \lambda) \quad (16)$$

$$\dot{\lambda} = - \frac{df(t, x, \lambda)}{dx}^T * \lambda \quad (17)$$

with boundary conditions

$$\mathbf{x}(t_0) = \mathbf{x}_0 \quad (18)$$

$$\mathbf{x}(t_f) = \mathbf{x}_f. \quad (19)$$

To make sure that this solution is indeed an optimal solution of the problem, we check whether the Legendre-Clebsch and Weierstrass conditions,

$$H_{uu} > 0 \quad \& \quad H(t, x, u_*, \lambda) > H(t, x, u, \lambda) \quad (20)$$

are satisfied. It can be shown that this is the case.

The BVP arising from the optimal control problem is solved using a collocation algorithm.

To get an idea about how the optimal Delta-V depends on the important parameters of the system, i.e., time-to-go, angle between the LOS of the initial and final target star, and the radius of the formation, we choose equally-spaced points on the sphere as the positions of the targets. We do this by using the method of equal area partitioning of a sphere developed by Leopardi.¹⁰ This allows us to make sure that we cover the whole phase space and save computation power, since the space space is represented by a minimum number of points.

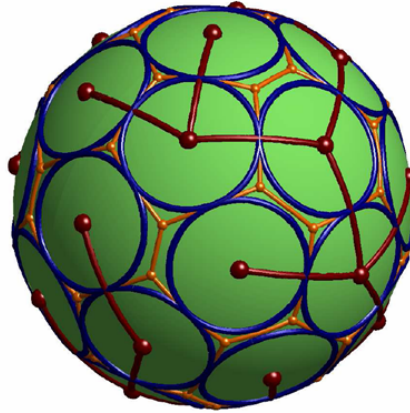


Figure 6. Equal partitioning of a unit sphere¹⁰

Using the optimization method developed above, we find the minimum Delta-V needed to go between these targets. In figure 7, the optimal Delta-V results from these millions of optimizations are averaged, giving Delta-V as an approximate function of Radius and LOS angle for a transfer time of 2 weeks.

In order to have a more realistic mission analysis, we used the top 100 TPF-C target stars,¹¹ and found the Delta-V for realignment between each target, as shown in figure 8.

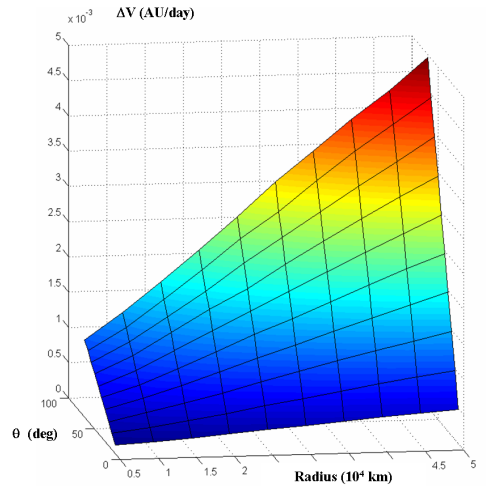


Figure 7. Surface of optimal Delta-V's as a function of distance from the telescope and angle between the LOS vectors of consecutively imaged stars ($\Delta t = 2$ weeks)

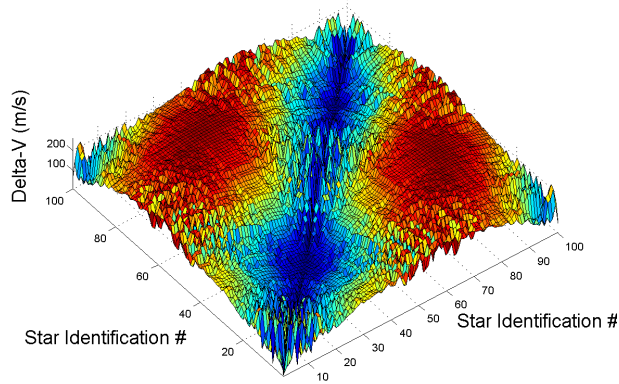


Figure 8. Minimum Delta-V needed to realign the occulter between the Top 100 TPF-C targets. The X and Y coordinates denote the identification number of the stars, and the Z coordinate denotes the minimum Delta-V to realign from X(i) to Y(j) in m/s.

3. The Continuous, Free-End Condition Case

Next, we consider the case where we know the initial state of the occulter at $t = t_0$ and we seek to find the minimum control target that resides on the two-dimensional occulter space in a given final time $t = t_f$. The Lagrangian and the differential equations are the same as before, but this time we employ a penalty function to ensure that the final state is in the occulter configuration space.

$$J = \frac{1}{\epsilon} \phi(x_f) + \int_{t_0}^{t_f} L(t, x, u) dt \quad (21)$$

$$(22)$$

The $\frac{1}{\epsilon} \phi(x_f)$ term weighs the constraint, which specifies that the occulter must be in the configuration space at the final time, very highly, thus ensuring that it is satisfied.

$$\phi(t_f) = [((x - x_h)^2 + (y - y_h)^2 + (z - z_h)^2 - R^2)^2 + (\dot{x} - \dot{x}_h)^2 + (\dot{y} - \dot{y}_h)^2 + (\dot{z} - \dot{z}_h)^2] \quad (23)$$

Proceeding as before, the 12-dimensional BVP is formed

$$\dot{x} = f(t, x, \lambda) \quad (24)$$

$$\dot{\lambda} = - \frac{df(t, x, \lambda)^T}{dx} * \lambda \quad (25)$$

with the following boundary conditions

$$\mathbf{x}(t_0) = \mathbf{x}_0 \quad (26)$$

$$\lambda(t_f) = \frac{1}{\epsilon} \frac{d\phi(t_f)^T}{dx} \quad (27)$$

This BVP is solved using collocation. After experimenting with some ϵ values, we found that $\epsilon = 0.01$ gives solutions that almost completely satisfy the constraint and the optimality. These results were checked against the point-to-point optimization case as well as a SQP method, giving almost perfect matches.

4. The Continuous, Open-End-Time Case

Finally, we consider the case where we know the initial state of the occulter at $t = t_0$ and we seek to find the minimum time trajectory that takes us to a final destination. Since the minimum time solution dictates that the maximum control is employed at all times, we simplify the problem by redefining the control

$$u = u_{max} * \begin{pmatrix} \sin(u_1) \\ \cos(u_1)\sin(u_2) \\ \cos(u_1)\cos(u_2) \end{pmatrix}. \quad (28)$$

Since our aim is to minimize time, the cost function becomes

$$J = \int_{t_0}^{t_f} 1 dt \quad (29)$$

Because the problem is open-end time, the Hamiltonian is not a function of time, and the final state is fixed, the Hamiltonian should be equal to zero at all times (See Bryson & Ho for details⁷).

$$0 = H(x, u, \lambda) \quad (30)$$

Solving the Hamiltonian constraint 30 along with the optimality conditions 32

$$0 = H_{u_1}(x, u, \lambda) \quad (31)$$

$$0 = H_{u_2}(x, u, \lambda) \quad (32)$$

for $\lambda_4, \lambda_5, \lambda_6$

$$\begin{pmatrix} \lambda_4 \\ \lambda_5 \\ \lambda_6 \end{pmatrix} = \begin{pmatrix} h_1(x, u, \lambda_1, \lambda_2, \lambda_3) \\ h_2(x, u, \lambda_1, \lambda_2, \lambda_3) \\ h_3(x, u, \lambda_1, \lambda_2, \lambda_3) \end{pmatrix} \quad (33)$$

derivating with respect to time and plugging in the solution from 25, we obtain

$$\begin{pmatrix} \dot{u}_1 \\ \dot{u}_2 \end{pmatrix} = \begin{pmatrix} f_1(x, u, \lambda_1, \lambda_2, \lambda_3) \\ f_2(x, u, \lambda_1, \lambda_2, \lambda_3) \end{pmatrix} \quad (34)$$

In an effort to be concise, we do not include the closed-form solution in this paper. The optimization problem now becomes a well-defined 12-dimensional BVP (6 state variables, 2 control variables and 3 adjoint-state variables, since $\lambda_4, \lambda_5, \lambda_6$ were eliminated, and one extra augmented-state variable for the unknown end-time, $\dot{t}_f = 0$), with 12 boundary conditions given in 27. Collocation algorithms do not perform well due to the singularity of the states. Shooting methods, however, would be able to solve this problem, provided we have a good initial guess. In the absence of good initial conditions, we had mixed results when using the indirect approach for the minimum-time problem. At times, the iterations did not converge to the solution, forcing us to rely on the slower direct method described above. These results can nevertheless be used to check the optimality of the SQP solutions. After finding the solution using SQP, it can be fed to the indirect method in order to check the optimality and to achieve high-order accuracy. Current work focuses on overcoming the convergence problem by separating the time domain in continuous sections.

In this problem, $x(t_f)$ is dependent on the flight time, since the position of the occulter is defined by the position of the telescope and the star location. To find the minimum time transfer problem, the following procedure is followed. First, we guess the t_f . Then, we integrate the equations of motion to find the location of the telescope and the star at that time. From the LOS requirement, we find $x(t_f)$, and we then solve the above-defined problem. If the minimum time guess is lower or higher than the obtained t_f , we continue iteration until the difference between the guess and the t_f from the optimization is negligible.

IV. The Time-Dependent Traveling Salesman Problem

After finding the relevant minimum-fuel trajectories between any given star-imaging sessions, the sequencing and timing of the imaging session is examined, in order to minimize global fuel consumption. The reflection of sunlight from the occulter to the telescope interferes with the imaging of the planetary system. This constrains the occulter to be approximately between 45 to 95 degrees from the Sun direction (See figure 9).

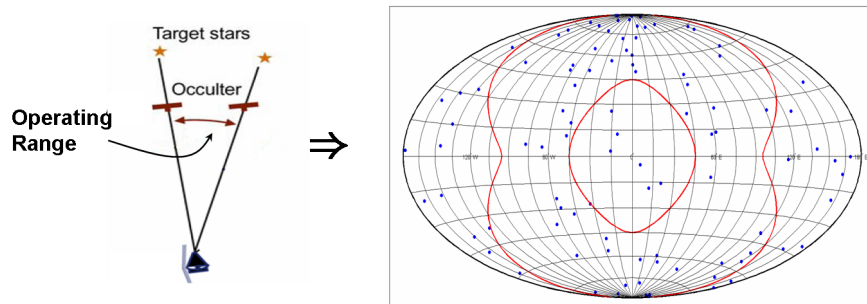


Figure 9. Operating range restriction of the occulter shown on a skymap

By including the constraints imposed by the telescoping requirements, the problem becomes a Time-Dependent Traveling Salesman Problem with dynamical constraints (See figure 10). The problem reduces to finding the minimum sum sequence that connects the rows and columns of the time-dependent TSP matrix. There are other constraints that we impose on the sequencing that are not shown on this figure. To ensure that the images of the planetary system of interest do not produce the same results, the minimum time between re-imaging of a target is 6 months. We randomly choose which stars are to be revisited, and how many times. While we do have the capability to ensure that there are no planets along the LOS, and to take into account the albedo effect of the Moon, we choose not to consider these minor constraints at this stage of optimization in order to save on computation.

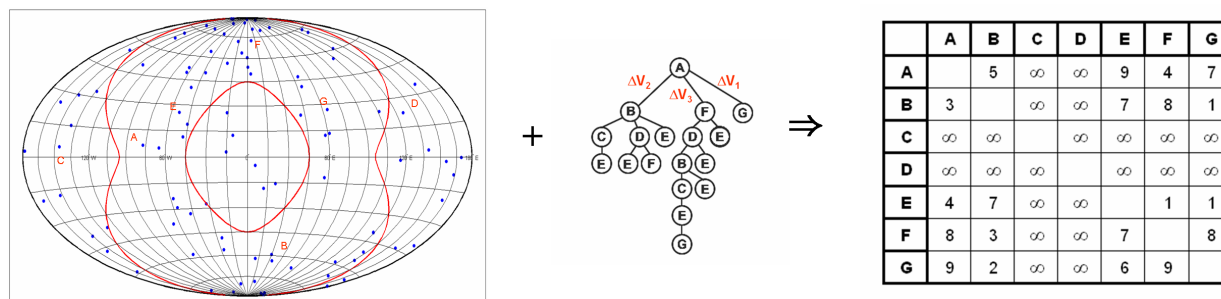


Figure 10. Including the constraints, the global optimization problem is converted to finding the best ordering of target stars, where the Delta-V's between the targets are shown on the time-dependent TSP matrix. In the figure, unaccessible zones are shown as ∞ .

In order to solve the global optimization problems, two heuristic, Tabu Search and Branch-And-Cut, methods were used. For problems of the size of our interest, the Tabu Search method¹² can find the best sequence for the no-constraint case very fast and very close to the optimal solution. However, it is not apparent how this method can be expanded to the case with dynamic constraints. The Branch-And-Cut algorithm, by contrast, can include constraints, but has a long computational time, and results may be far from optimal. We adopted a combined approach, using both methods, to enhance the solution of the TSP problem at hand. We started by solving the TSP problem via Tabu Search, each time assuming that constraints are fixed for all time, meaning that a target in a restricted zone is assumed to be permanently unobservable, even if that target will be visitable in several months' time. Patching the solutions we obtain from the Tabu Search, we formulate an initial guess for the optimal sequence, which we then feed to the Branch-And-Cut algorithm. A sample solution to the TSP using this methodology is shown in figure 11.

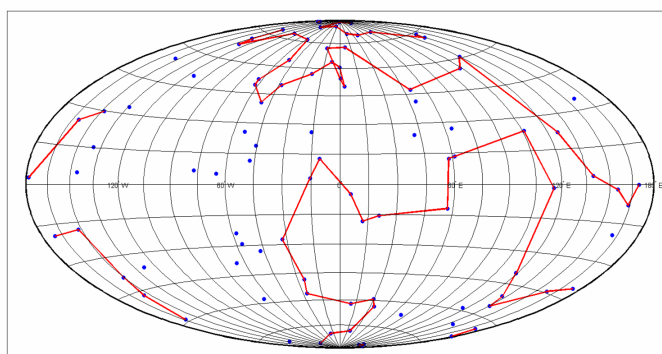


Figure 11. Global optimal solution to the single occulter TSP for 75 imaging sessions of the Top 100 TPF-C stars, with 2 weeks flight time between targets and no revisiting

The algorithms developed so far enable us to find the total minimal Delta-V requirement for a given mission. Figure 12 shows the averaged Delta-V obtained for the TPF-C top 100 stars, where we randomly picked which stars were to be revisited more than once as a function of the size of the formation and the average realignment time.

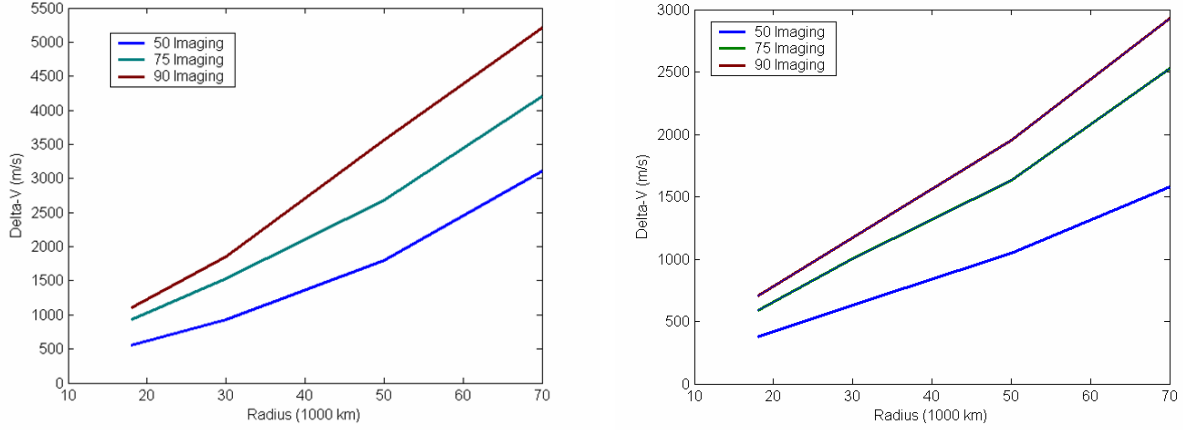


Figure 12. Minimum total Delta-V curves for the single occulter mission (Left: $\Delta t = 1$ week, Right: $\Delta t = 2$ weeks).

Table 1. Maximum thrust needed for the minimum control effort solutions obtained in figure 12

Radius	Max Thrust
18,000 km	18 mN ($\sim 0.05 \text{ mm}/s^2$)
30,000 km	31 mN ($\sim 0.10 \text{ mm}/s^2$)
50,000 km	52 mN ($\sim 0.15 \text{ mm}/s^2$)
70,000 km	70 mN ($\sim 0.2 \text{ mm}/s^2$)

V. A Feasibility Study: Performance of the SMART-1 Spacecraft as an Occulter

For a concrete understanding of the feasibility of the mission, the performance of an example spacecraft, SMART-1, as an occulter, is analyzed. SMART-1 is a spacecraft designed by ESA equipped with a solar-powered Hall-effect thruster.¹³ For this study, we used the top 100 TPF-C targets and the exact specifications of the SMART-1 spacecraft, given in table 2.

Table 2. Specifications of the SMART-1 spacecraft

Maximum Thrust	68 mN
Mass Ratio	0.83
Propellant Mass	80 kg
Total Delta-V	3600 m/s
Isp	1640 s
Maximum Acceleration	$0.2 \text{ mm}/s^2$
Full Thrust Life Time	210 days

Figure 13 shows the results obtained if we employ a minimum control effort strategy. We can see from this figure that as the time between the imaging sessions are decreased, the total number of observations that can be done decreases as well. And as the radius of the formation increases, number of imaging session decreases.

Figure 14 shows the results obtained if we employ a minimum-time transfer strategy. We can see from this figure that, as the radius of the formation increases, the number of imaging session decreases. Comparing this with figure 14, it is apparent that the minimum-time strategy trades off speed of observations against

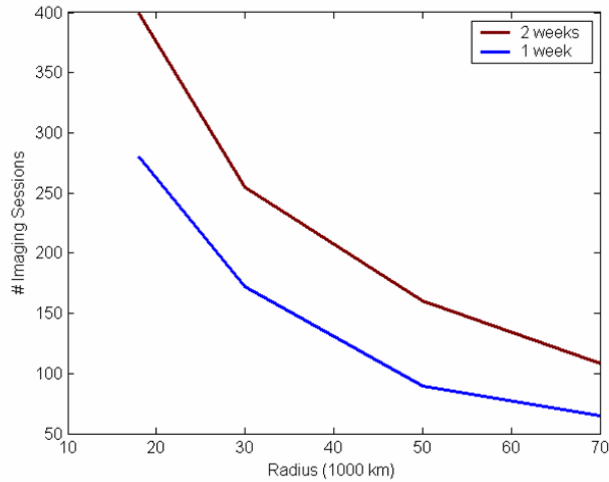


Figure 13. Number of stars imaged versus radius with control optimized for control effort (with Smart-1 capabilities).

the number of total observations.

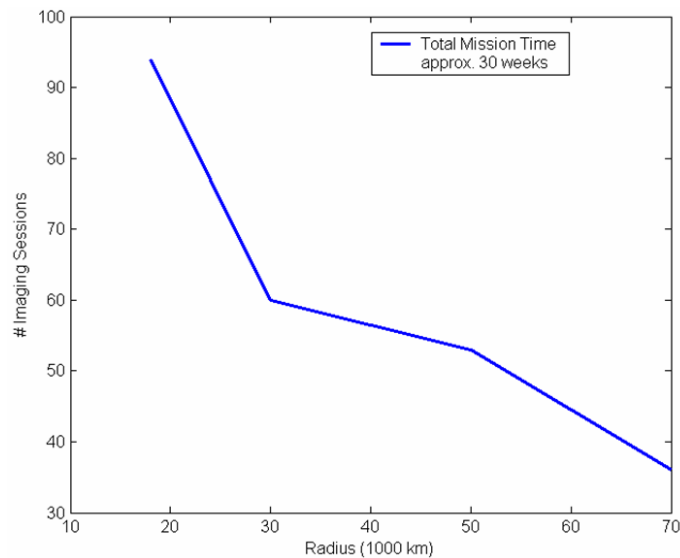


Figure 14. Number of stars imaged versus radius with control optimized for minimum time (with Smart-1 capabilities).

Looking at these comparisons, it is apparent that, notwithstanding the difficulties involved, the mission is within the reach of the current technology. With the next generation thrusters, it should be possible to maneuver the approximately 30 meter diameter occulter to do enough imaging to be able to find earthlike planets.

VI. Conclusions

A methodology is outlined to find the optimal configuration of a satellite formation, consisting of a telescope and an occulter around the Sun-Earth L2 Halo orbits, for the imaging of extra-solar planets. Trajectory optimization of the occulter motion between imaging sessions of different stars was performed and results from different methods of optimization were compared. This enabled the transformation of the global optimization problem into a dynamically constrained Time-Dependent TSP. This problem was

solved by employing heuristic methods. For a concrete understanding of the feasibility of the mission, the performance of an example spacecraft, SMART-1, as an occulter, was analyzed. A trade-off study of cost and scientific achievement, for different control techniques and configurations, will be completed as part of future research.

References

- ¹Vanderbei, R. J., Spergel, D. N., and Kasdin, N. J., "Circularly Symmetric Apodization via Starshaped Masks," *The Astrophysical Journal*, Vol. 599, 2003, pp. 686.
- ²Vanderbei, R. J., Spergel, D. N., and Kasdin, N. J., "Spiderweb Masks for High-Contrast Imaging," *The Astrophysical Journal*, Vol. 590, 2003, pp. 593.
- ³Cash, W., "Detection of Earth-like planets around nearby stars using a petal shaped occulter," *Nature*, , No. 442, July 2006, pp. 51–53.
- ⁴Kolemen, E. and Kasdin, N. J., "Optimal Configuration of a Planet-Finding Mission Consisting of a Telescope and a Constellation of Occulters," January 2007, AAS 07-202.
- ⁵Kolemen, E., Kasdin, N. J., and Gurfil, P., "Quasi-Periodic Orbits of the Restricted Three Body Problem Made Easy," *Proceedings of the New Trends in Astrodynamics and Applications*, August 2006.
- ⁶Standish, E., "JPL Planetary and Lunar Ephemerides, DE405/LE405," *JPL IOM*, Vol. 312.F-98-048, 1998.
- ⁷Bryson, A. E. and Ho, Y. C., *Applied Optimal Control*, Hemisphere Publishing Corp., New York, 1975.
- ⁸Vanderbei, R. J., "LOQO: An interior point code for quadratic programming," *Optimization Methods and Software*, Vol. 11, 1999, pp. 451–484.
- ⁹Wächter, A. and Biegler, L. T., "Line Search Filter Methods for Nonlinear Programming: Motivation and Global Convergence," *SIAM Journal on Optimization*, Vol. 16, No. 1, 2005, pp. 1–31.
- ¹⁰Leopardi, P., "A partition of the unit sphere into regions of equal area and small diameter," *Electronic Transactions on Numerical Analysis*, Vol. 25, 2006, pp. 309–327.
- ¹¹<http://sco.stsci.edu/roses/index.php>, Top 100 TPF-C Targets.
- ¹²Glover, F. and Laguna, M., *Tabu Search*, Kluwer Academic Publishers, Norwell, MA, 1997.
- ¹³<http://www.esa.int/SPECIALS/SMART-1>, The official SMART-1 website.